Electronic Supplementary Information (ESI)

Heterojunction engineering of graphitic carbon nitride (g-C_3N_4) *via* Pt loading with improved daylight-induced photocatalytic reduction of carbon dioxide to methane

Wee-Jun Ong, Lling-Lling Tan, Siang-Piao Chai* and Siek-Ting Yong

Multidisciplinary Platform of Advanced Engineering, Chemical Engineering Discipline, School of Engineering, Monash University, Jalan Lagoon Selatan, Bandar Sunway, 47500 Selangor, Malaysia.

* Corresponding author.

Tel: +603-5514 6234; Fax: +603-5514 6207

E-mail address: chai.siang.piao@monash.edu

(1) Light spectrum of daylight bulb used in photocatalytic experiments

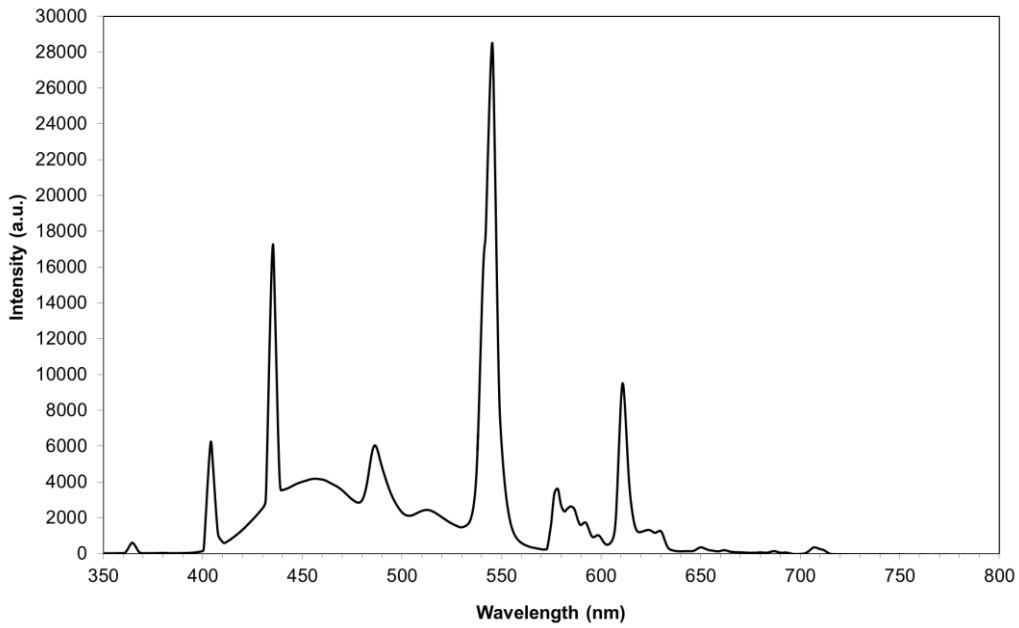

Fig. S1 Light spectrum of the low-power 15 W energy-saving daylight lamp (Philips, TORNADO 15 W WW E27 220–240 V 1CT).

(2) Particle size distribution of Pt/CN hybrid nanostructures

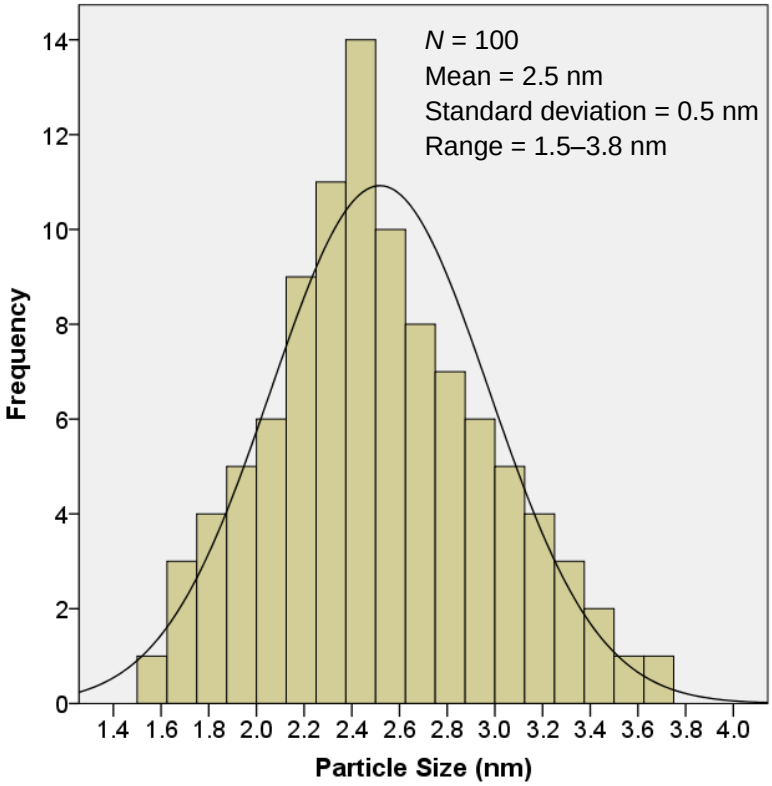

Fig. S2 Particle size distribution of Pt nanoparticles decorated on the g-C_3N_4 sheets. The average diameter (± standard deviation) of Pt nanoparticles was 2.5 (± 0.5 nm), calculated by counting the diameter of 100 individual Pt nanoparticles from the STEM images.

(3) TGA plots of the as-developed photocatalysts

TGA was performed to determine the loading of Pt present in the Pt/CN hybrid nanocomposites. Fig. S3 shows the TGA curves of pure g-C_3N_4 and Pt/CN samples. The decomposition of g-C_3N_4 started at *ca*. 520 ^oC and was completed at *ca*. 620 ^oC in pure g-C_3N_4. The weight loss region could be observed for all the Pt/CN hybrid systems. The residual weight percentage of 0.5Pt/CN, 1Pt/CN, 2Pt/CN, 5Pt/CN and 10Pt/CN hybrid nanostructures were found to be *ca*. 0.5, 1, 2, 5 and 10 wt%, respectively, which were considered to be the Pt contents in the Pt/CN nanocomposites. Generally, these values were well-corresponded to the theoretical estimation of Pt doping onto the g-C_3N_4 sheets.

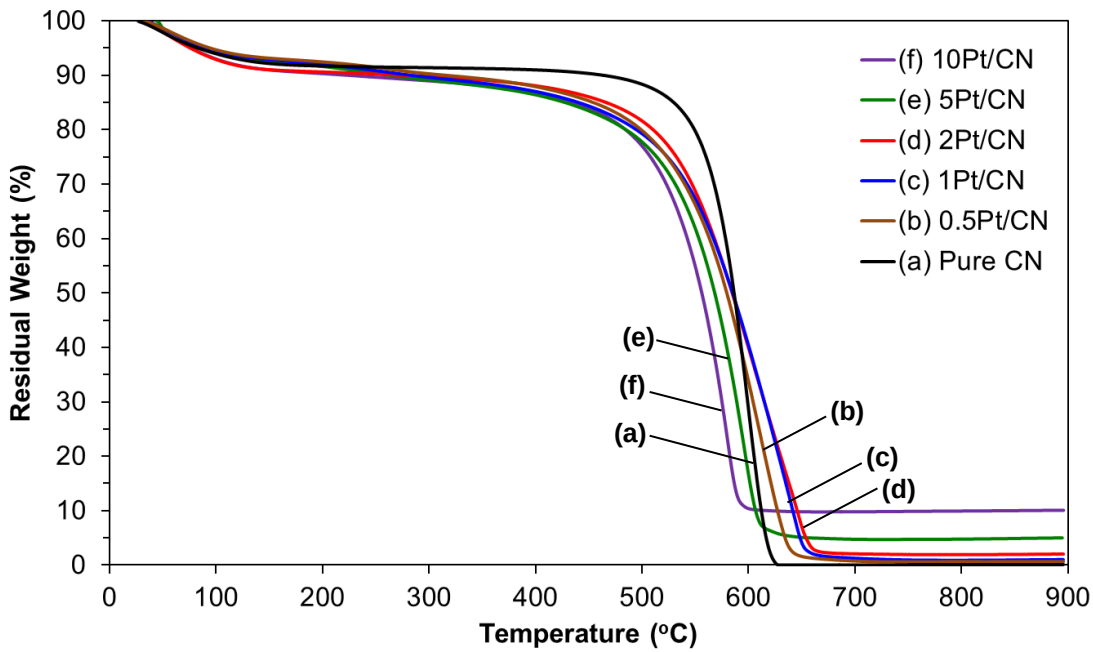

Fig. S3 TGA curves of pure g-C_3N_4 and Pt/CN samples.

(4) Raman spectra of the as-developed photocatalysts

As depicted in Fig. S4, no distinct variations in the Raman peaks could be observed for all the Pt/CN samples, implying that the Pt loading has little influence on the molecular skeleton and lattice structure of g-C_3N_4. The typical characteristic peaks of g-C_3N_4 at 460, 588, 703, 740, 975, 1115, 1145, 1233, 1460 and 1620 cm^{-1} were observed, which matched well with the previous published reports.[1-5] The sharp peaks at 703 and 975 cm^{-1} evidenced the existence of a heptazine ring structure.[6] The peak at 703 cm^{-1} was ascribed to the in-plane bending vibrations of the heptazine linkages, whereas the 975 cm^{-1} peak was assigned to the symmetric N-breathing mode of heptazine units.[7] In addition, the broad and asymmetric peaks ranging from 1300 to 1700 cm^{-1} were attributed to the stretching vibrations of C–N and analogues to the typical "D" and "G" bands found in the graphitic carbon-based nanomaterials.[8] The Raman results of the pure g-C_3N_4 and Pt/CN samples were in accordance with the FTIR results, elucidating the successful formation of g-C_3N_4 and that the basic framework of g-C_3N_4 remained unaltered despite being loaded with Pt metals.

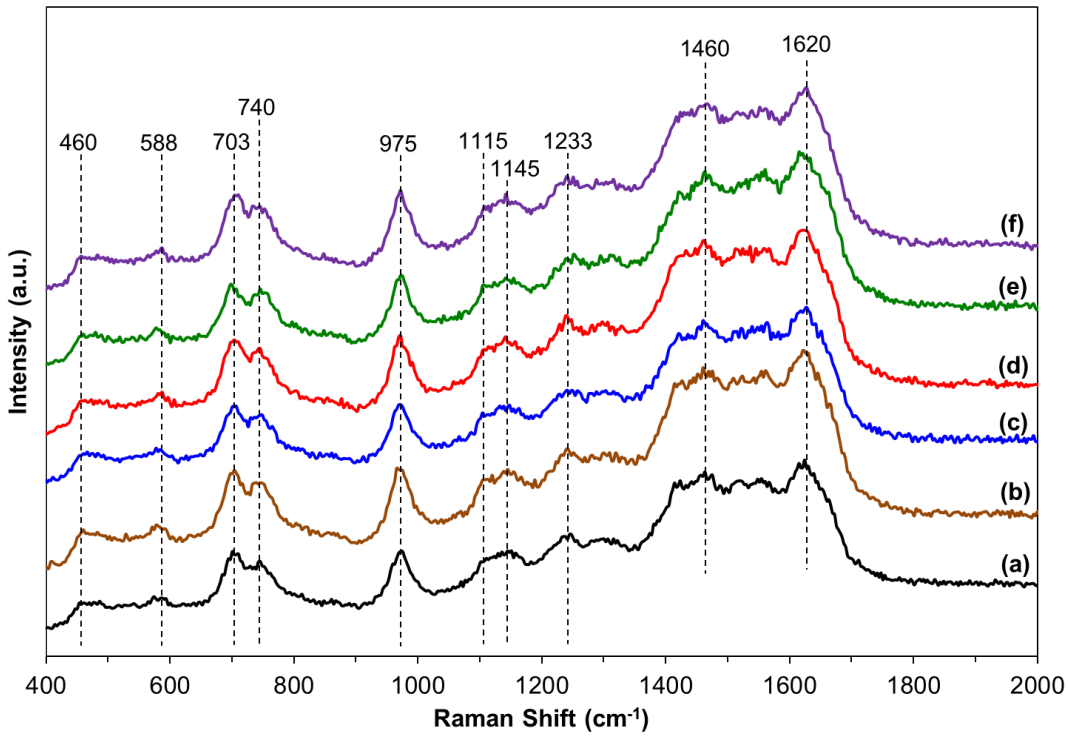

Fig. S4 Raman spectra of (a) pure g-C_3N_4, (b) 0.5Pt/CN, (c) 1Pt/CN, (d) 2Pt/CN, (e) 5Pt/CN and (f) 10Pt/CN hybrid nanocomposites.

(5) Control measurements of the photocatalytic reduction of CO_2

To better understand the mechanistic pathway of CH_4 formation, we have performed a series of background experiments under the following conditions: (1) without light irradiation in a flow of CO_2 and H_2O vapor, (2) under N_2 and H_2O vapor flow, (3) under CO_2 flow only without H_2O vapor, and (4) under CO_2 and H_2O vapor flow in the absence of photocatalysts. In all cases, no appreciable CH_4 gas was detected (Fig. S5). These background tests clearly confirmed that the CH_4 yield observed stemmed from the photocatalytic reduction of CO_2, and not from the photodecomposition of organic residues on the catalyst surface. This concludes that reactant feeds (CO_2 and H_2O) and visible light source are indispensable for the photocatalytic process, which are consistent with our previous reported studies.[9-11]

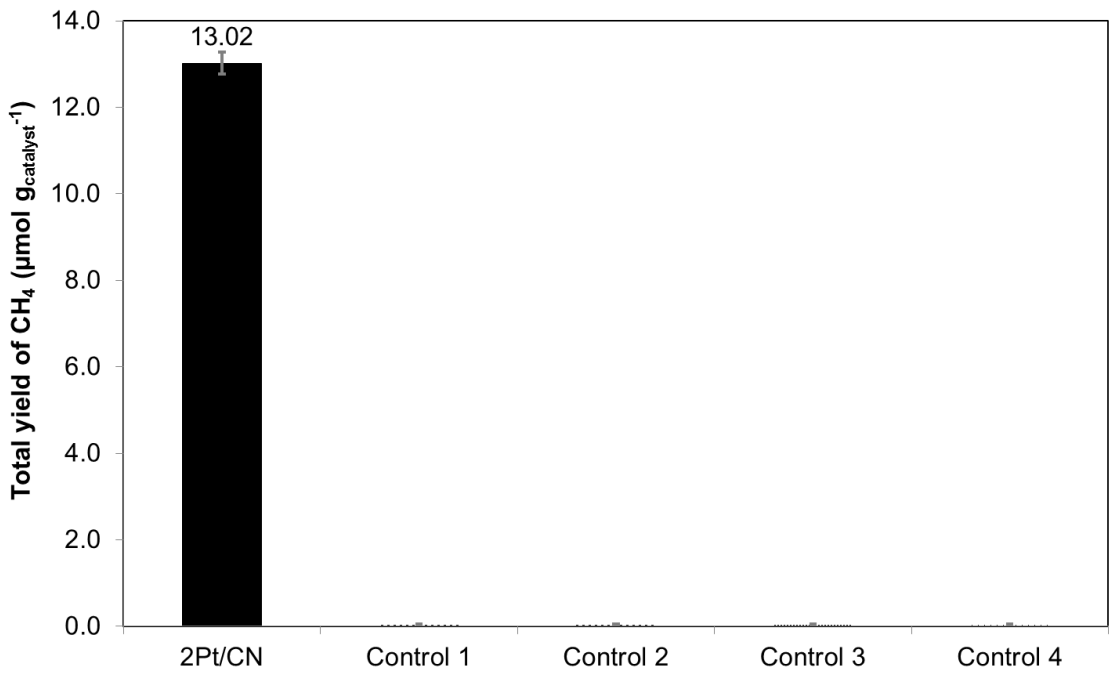

Fig. S5 Total yield of CH_4 over pure g-C_3N_4 and Pt/CN samples under visible light irradiation. Control experiments performed under four different conditions: (Control 1) without light irradiation in a flow of CO_2 and H_2O vapor, (Control 2) N_2/H_2O flow, (Control 3) CO_2 flow without H_2O vapor, and (Control 4) CO_2/H_2O flow without photocatalysts were included.

Supplementary References

1 X. Bai, L. Wang, Y. Wang, W. Yao and Y. Zhu, *Appl. Catal., B*, 2014, **152–153**, 262-270.

2 Q. Xiang, J. Yu and M. Jaroniec, *J. Phys. Chem. C*, 2011, **115**, 7355-7363.

3 Y. Hou, Z. Wen, S. Cui, X. Guo and J. Chen, *Adv. Mater.*, 2013, **25**, 6291-6297.

4 Y. Chen, J. Li, Z. Hong, B. Shen, B. Lin and B. Gao, *Phys. Chem. Chem. Phys.*, 2014, **16**, 8106-8113.

5 D. Hollmann, M. Karnahl, S. Tschierlei, K. Kailasam, M. Schneider, J. Radnik, K. Grabow, U. Bentrup, H. Junge, M. Beller, S. Lochbrunner, A. Thomas and A. Brückner, *Chem. Mater.*, 2014, **26**, 1727-1733.

6 S. Tonda, S. Kumar, S. Kandula and V. Shanker, *J. Mater. Chem. A*, 2014, **2**, 6772-6780.

7 B. Long, J. Lin and X. Wang, *J. Mater. Chem. A*, 2014, **2**, 2942-2951.

8 X. Bai, R. Zong, C. Li, D. Liu, Y. Liu and Y. Zhu, *Appl. Catal., B*, 2014, **147**, 82-91.

9 W.-J. Ong, L.-L. Tan, S.-P. Chai, S.-T. Yong and A. R. Mohamed, *Nano Res.*, 2014, **7**, 1528-1547.

10 W.-J. Ong, M. M. Gui, S.-P. Chai and A. R. Mohamed, *RSC Adv.*, 2013, **3**, 4505-4509.

11 L.-L. Tan, W.-J. Ong, S.-P. Chai and A. R. Mohamed, *Chem. Commun.*, 2014, **50**, 6923-6926.